Chinese Chemical Letters 34 (2023) 107753

Contents lists available at ScienceDirect

Chinese Chemical Letters

journal homepage: www.elsevier.com/locate/cclet

Integrated and dual-responsive lipopeptide nanovector with parallel effect to tumor and micro-environment regulation by efficient gene and drug co-delivery

Xiaobing Chen[a,1], Huan Yang[a,1], Xu Song[a,1], Hong Liang[a,c], Yu Wei[a], Jiao Lu[a], Matthias Barz[b], Rongrong Jin[a,*], Yu Nie[a,*]

[a] National Engineering Research Center for Biomaterials, Sichuan University, Chengdu 610064, China
[b] Leiden Academic Center for Drug Research (LACDR), Leiden University, Leiden 2333 CC, The Netherlands
[c] Department of Pharmacy, Sichuan Academy of Medical Sciences & Sichuan Provincial People's Hospital, School of Medicine, University of Electronic Science and Technology of China, Chengdu 610072, China

ARTICLE INFO

Article history:
Received 20 April 2022
Revised 13 August 2022
Accepted 16 August 2022
Available online 24 August 2022

Keywords:
Gene delivery
Integrated co-delivery
Dual-responsive
Lipopeptide
Tumor micro-environment regulation

ABSTRACT

The integrated lipopeptide (RVA)/gene complexes are fabricated with bi-directional regulation on tumor cells and micro-environment. After self-assembling and target coating modification, the poly(γ-glutamic acid) (γ-PGA)/RVA nano-vectors can sequentially respond to pH & redox stimuli, and guarantee efficient therapeutic gene delivery and control release of all-*trans* retinoic acid. The design provides a facile but promising strategy to treat refractory cancers.

Gene therapy is becoming a crucial tool for the genetic disease treatment and vaccine- based pandemics prevention, providing more options for pathema that cannot be addressed by conventional therapies [1,2]. Replacing, correcting or removing the oncogene of tumor cell is the general treatment for cancer therapy [3]. However, directing against tumor cell alone is less effective, as the educated tumor microenvironment (TME) often help tumor deteriorate and evade immune surveillance [4,5]. Pancreatic cancer is a very typical solid tumor with complicated external environment, which always lead to a high rate of relapse after conventional treatment and oncogenes knockout therapy (*e.g.*, Kras and TP53) [6].

TME is generally a redox disordered and acidic system with tumor associated macrophages and fibroblasts infiltration, which protect tumor from drug killing and form a vicious circle with tumor growth [7–9]. Thus, a parallel strategy that combines tumor inhibition with TME regulation is exploring for overcoming refractory cancers. For example, co-delivery of two drugs (paclitaxel and marimastat) showed a completely suppressed metastasis of breast cancer. The paclitaxel inhibited malignant proliferation of tumor cells while marimastat reduced activity of matrix metalloproteinase in TME [10]. Another successful combination was gemcitabine and all-*trans* retinoic acid (ATRA) for treatment of pancreatic cancer.

The ATRA could remodel the complex dense extracellular matrix by reducing connective tissue, thus improved chemotherapeutics of gemcitabine penetration into the tumor tissues. As a result, the killing effect of gemcitabine on tumors is enhanced by ~50% [11,12]. Our group also confirmed that a ferric oxide gene delivery system with M1 polarization of tumor associated macrophages and tumor growth inhibition by Fenton effect, shows much satisfactory *in vivo* efficacy on breast cancer therapy [13].

While, the accumulation of multiple functions in one delivery system usually complicates the components and structure of gene nanocarriers. Facile and reasonable design without compromising therapeutic effect is demanded. Recently, integrated fabrication of low molecular drug as prodrug carrier provides a good reference [14–16]. Our group also tried to integrate fluorescence probes in gene delivery vehicles for *in vivo* imaging and tracing [17]. Advances of these integrations include high loading capacity, better controllable release, more accurate tracing and facile formulation preparation [18]. In addition, some TME-responsive design in ve-

* Corresponding authors.
E-mail addresses: jinrr2015@scu.edu.cn (R. Jin), nie_yu@scu.edu.cn (Y. Nie).
[1] These authors contributed equally to this work.

https://doi.org/10.1016/j.cclet.2022.107753
1001-8417/

hicles could also promote delivery efficiency [19–21]. Pinpointed cascading design (based on pH-, redox-, or enzyme-response) and targeting decoration has confirmed to promote gene expression by orders of magnitude in our previous studies [17,22,23]. With our continuing interests in facile integrated nanomaterials for tumor gene therapy, we believe that efficient co-delivery of gene and drug by integrated drug carrier should be considered, and a "sequential" response design to TME (such as pH and redox) in the carrier might also benefit for the delivery.

Herein, based on the established lipopeptides platform [24–26], we designed and synthesized an upgraded gene delivery system the poly(γ-glutamic acid)/integrated lipopeptide (γ-PGA/RVA), aiming at achieving parallel effect on tumor and TME regulation, with pH & redox dual-response. Prodrug of all-*trans* retinoic acid (ATRA) was used as the hydrophobic part of carrier, as it has effects on TME regulation [27]. The cationic dendritic arginine was developed as the hydrophilic part for aggregation of nucleic acid, while a disulfide bond was used to connect these two moieties for the following self-assembly. After sequential addition of gene and γ-PGA by electrostatic action, the γ-PGA/RVA/gene complexes were formed. The outer γ-PGA layer can specifically combine to gamma-glutamyl transpeptidase (GGT) overexpressed on the surface of tumor cells, and induce cellular entry of particles. Under the acidic lysosomal conditions, γ-PGA changed its conformation and falls from the RVA/gene complexes, which facilitates the following lysosome escape and cytoplasm entry of therapeutic gene. In the reductive cytoplasm, gene complexes are disintegrated due to break of disulfide bonds. The released gene and prodrug consequently exert their individual and synergistic impact on treatment [28,29]. As a proof-of-concept, reporter siRNA was used to verify the transfection efficiency, and siMMP-9 and siKras were selected to evaluate cure efficacy in the treatment of pancreatic cancer (Scheme 1) [30,31].

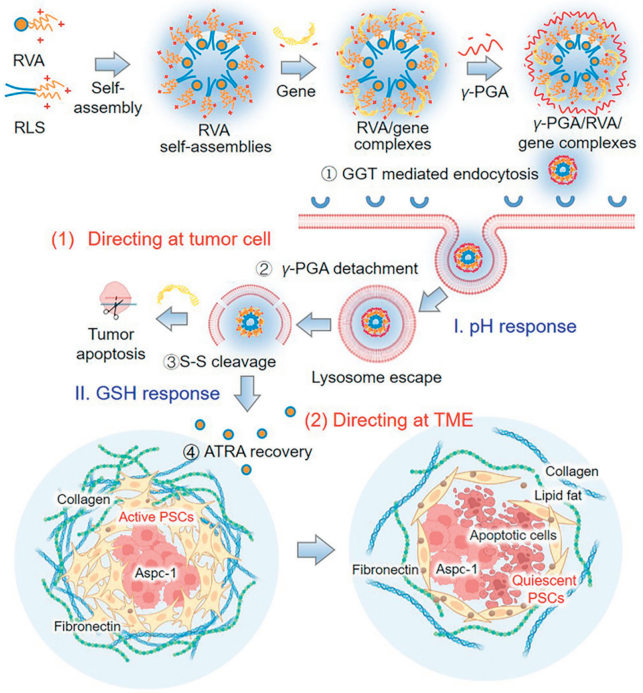

Scheme 1. Construction of integrated lipopeptide nanovector (γ-PGA/RVA/siRNA complexes) with parallel effect on both tumor and micro-environment regulation for tumor gene therapy. The hydrophilic part with arginine-rich coronary structure ensures efficient delivery of therapeutic gene, and hydrophobic core of all-*trans* retinoic acid is directed to restore the resting state of extracellular matrix. During delivery process, γ-PGA and disulfide bonds sequentially responds to specific pH and glutathione (GSH) conditions.

The chemical structure of ATRA integrated dendritic lipopeptides (RVA) and its related characterization is shown in Fig. 1 [32,33]. The characteristic peaks of hydrophobic ATRA at δ 1.05 (-CH_3), cystamine's peaks at δ 2.51-3.03 (m, -CH_2CH_2-) and peaks of arginine dendritic molecule (compound **2** in Fig. 1A) at δ 2.95, 3.14 (-$NHCH_2$-) all appeared in the ^{1}H NMR spectrum of RVA (Fig. 1B). Meanwhile, the result of matrix-assisted laser desorption/ionization time-of-flight mass spectrometry (MALDI-TOF MS) also confirmed the successful integration ($[M+H]^+ = 875.70$, Fig. 1C), agreed well with the theoretical molecular weight ($[M+H]^+ = 875.25$). In order to fabricate nano-scaled gene complexes, we mixed RLS [24] and RVA with a molar ratio of 5:1 (Fig. S1 in Supporting information), and prepared the RVA self-assemblies by common injection method. The Z-average diameter of obtained particles was 220.5 nm with zeta potential of +41.5 mV (Fig. 2A).

The cationic RVA self-assemblies were then sequentially co-incubated with anionic siRNA and γ-PGA to form binary (RVA/siRNA) and ternary (γ-PGA/RVA/siRNA) gene complexes. Optimal N/P ratios were screened by the dynamic light scattering (DLS) investigation on particle size and zeta potential (Fig. 2A). Results showed that by N/P ratio increasing from 10 to 40, size of the complexes fluctuated between 186 nm to 220 nm, and zeta potential was in the range of 38 mV to 44 mV. While at lower N/P of 5, size of complexes was very large (~807 nm), which was probably caused by the poor compressing capacity of RVA self-assemblies. After some preliminary experiments, RVA/siRNA binary complexes with N/P of 30 were selected for the following incubation with the targeting motif of γ-PGA (Fig. S1) [24]. The modification of negatively charged γ-PGA decreased zeta potential in a dosage-dependent mode, showing -36 mV at weight ratio of 5 (γ-PGA: siRNA) (Fig. 2B). The γ-PGA/RVA/siRNA complexes was dispersed in the medium containing 10% fetal bovine serum to study its stability under physiological conditions (Fig. 2C). The results showed that the particle size of γ-PGA/RVA/siRNA complexes is around 200 nm and remain unchanged within 5 d, while the zeta potential is also maintaining stability during the test. It indicates that the complexes of γ-PGA/RVA/siRNA has good stability under physiological conditions. Morphology of RVA assemblies and γ-PGA/RVA/siRNA complexes exhibited globular grain by transmission electron microscopy (TEM) observation with an average diameter ~75 and 125 nm, respectively (Figs. 2D and E). From the agarose gel electrophoresis evaluation, RVA assemblies were able to completely compress siRNA at N/P ratios higher than 6 (Fig. 2F). Adding of negatively charged γ-PGA did not disturb the condensation capacity (Fig. 2G) [34]. In the tumor mimicking microenvironment (5 mmol/L glutathione solution, GSH), migration bands of siRNA could be observed in RVA/siRNA complexes (Fig. 2F). This GSH responsiveness indicated a redox sensitive release instinct of RVA gene complexes [35]. In addition, the release of ATRA at different concentrations was measured by an ultraviolet spectrophotometer at 365 nm and a standard curve for ATRA release was plotted (Fig. 2H), as well as the release of ATRA in the RVA assembly in PBS and GSH (5 mmol/L) conditions. When PBS was used alone, the release of ATRA was markedly slow, with a 48 h cumulative release rate of only 20.76% (Fig. 2I). In contrast, the release of ATRA under GSH condition was significantly accelerated, indicating a supersensitive reaction of the disulfide bonds with cumulative release of 67.15% after 48 h.

Followingly, we evaluated the gene delivery efficiency of each step on Aspc-1 (pancreatic adenocarcinoma cells) and PSCs (pancreatic stellate cells) by Cy3 labeled siRNA complexes. First step was the cell membrane penetration process. After treatment with Cy3-siRNA loaded RVA or γ-PGA/RVA, cells were subjected to the confocal laser scanning microscopy (CLSM) observation. Significant

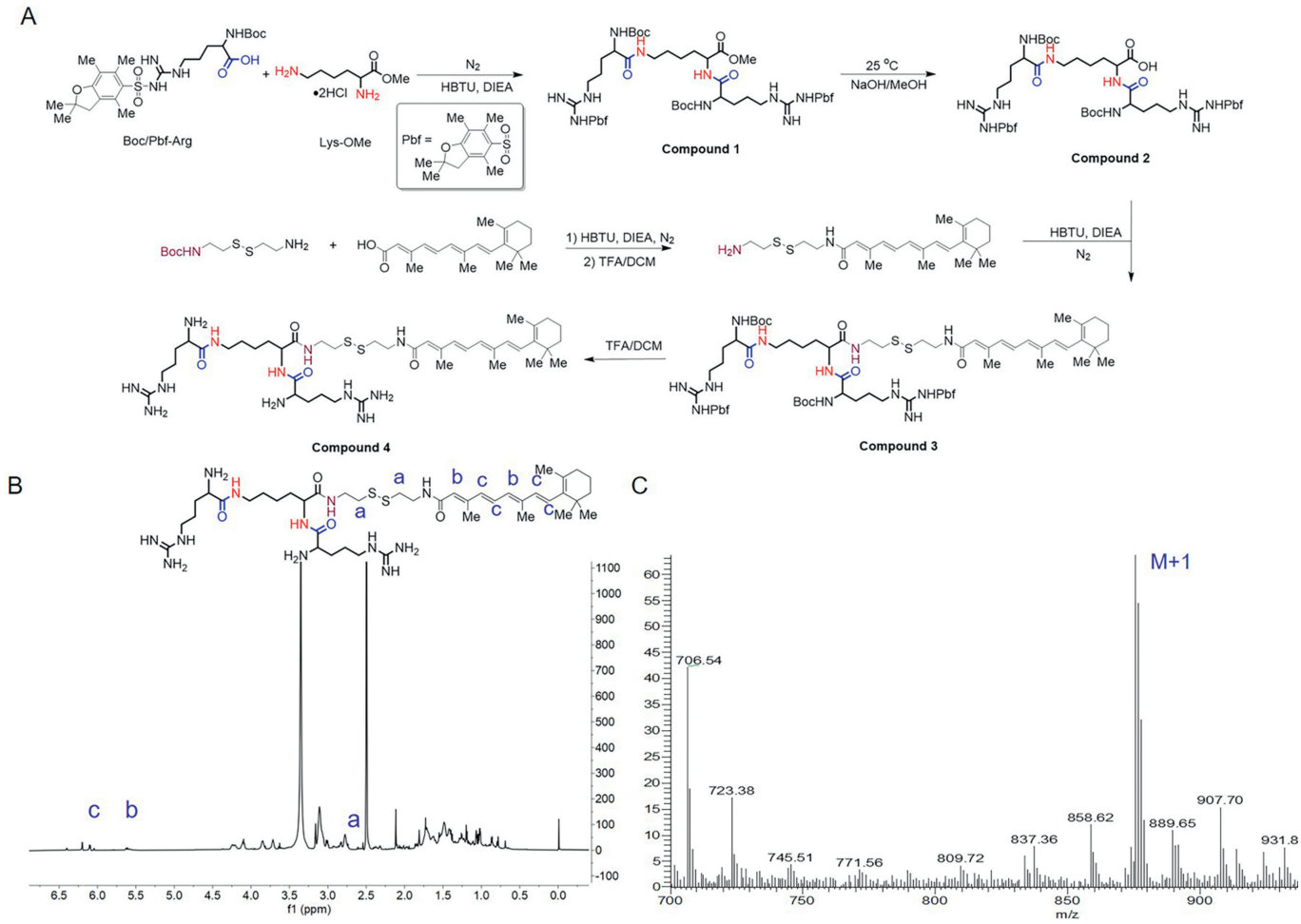

Fig. 1. The chemical synthetic route and characterization of all-*trans* retinoic acid-based siRNA delivery compound (RVA). (A) Chemical synthetic route. (B) ^{1}H NMR spectrum and (C) MALDI-TOF MS characterization of RVA.

difference between complexes with or without γ-PGA coating was detected at 0.5 h in PSCs cells (Figs. 3A and B), that γ-PGA enhanced the cellular uptake efficiency from 45% to 60%. While, no significant difference was detected in Aspc-1 cells. The difference is possibly due to the different GGT expression levels on these two cell types [36].

The intracellular fate of γ-PGA/RVA/siRNA complexes were investigated next, with expectation of environment triggered responses. pH sensitive disassociation of γ-PGA from the gene complexes was evaluated by fluorescence resonance energy transfer (FRET) phenomenon through CLSM observation (Fig. 3C) [37]. Fluorescence from FITC labeled γ-PGA (green) could work as donor, and the Cy3 labeled siRNA (red) was the acceptor. When the γ-PGA coating was closely interacted with RVA/siRNA core, the FRET phenomenon could be obvious. While, once the coating dropped off under acidic condition of lysosome, signal of FRET might gradually weaken. Because the distance between the fluorescent donor molecules of FITC and acceptor Cy3 would no longer meet the condition of FRET (<10 nm) [38].

As expected, at the beginning (first 2 h), all observed fluorescence points were yellow and orange-red, and the superimposed signal was originated from FRET. After 4 h co-incubation, both FITC signal and FRET-mediated Cy3 signal enhanced, due to increased cellular uptake of gene complexes. Meanwhile, some single FITC green fluorescent dots began to appear, although most of the FITC and FRET-mediated Cy3 signals were overlapping. It suggested that a portion of FITC-γ-PGA was dissociated from the ternary gene complexes. At this time, the distance between some FITC molecules and Cy3 no longer met the condition of FRET [37,39], resulting in decrease of FRET-mediated Cy3 signal and increase of green fluorescence signal from FITC. Over time, more single FITC green spots could be observed (at 6 h), whereas the fluorescence intensity of FRET-mediated Cy3 attenuated gradually. Through the calculation, the FRET efficiency of FITC-γ-PGA/RVA/Cy3-siRNA complexes decreased from 99.3% (2 h) to 73.4% (6 h) (Fig. 3D).

Next, whether this pH induced de-shielding could benefit for lysosomal escape and intracellular distribution was investigated, with incubation of FITC-γ-PGA(green)/RVA/Cy5-siRNA(red) gene complexes on Aspc-1 cells for 6 h. Lysosome was stained with Lysotracker Red, and set to be a blue pseudo-color in the following fluorescence co-localization experiments (Fig. 3E). During early period of time (2 h, without de-shielding of γ-PGA), fluorescence signal was cyan (green and blue superposition) and even white (red, green and blue superposition), due to a large number of gene complexes retention in lysosome. 4 h later, when the signal of FITC was highly overlapped with the signal of thelysosome (showing cyan), red fluorescent spots from RVA/Cy5-siRNA binary complexes appeared. It indicated that when the γ-PGA gradually dropped off (Figs. 3E and F), it was retained in the lysosome. Meanwhile, some of RVA/Cy5-siRNA binary complexes started to realize lysosomal escape, and more red fluorescent spots were observed after 6 h incubation. The co-localization evaluation by Pearson correlation (Rr) calculation (Fig. 3F) also confirmed the difference [40]. Rr of fluorescence from Cy5-siRNA (red) and lysosome (blue) were reduced

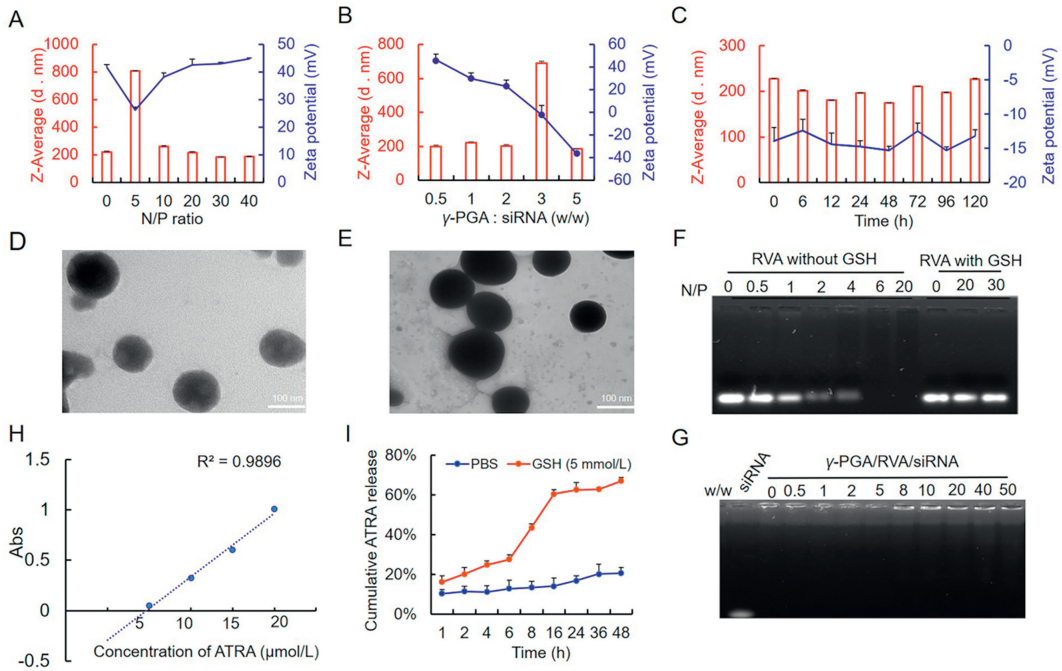

Fig. 2. Physicochemical characterization of gene complexes (RVA/siRNA binary and γ-PGA/RVA/siRNA ternary complexes) in the prepared reductive conditions. (A) Size and zeta potential of RVA/siRNA binary complexes at varied N/P ratios. (B) Size and zeta potential of γ-PGA/RVA/siRNA ternary complexes (N/P 30) with varied γ-PGA/siRNA weight ratios. (C) Size and zeta potential changes of γ-PGA/RVA/siRNA complexes (N/P 30, siRNA 3 μg) under physiological conditions. (D) Morphology observation of optimized RVA assemblies and (E) γ-PGA/RVA/siRNA complexes (N/P 30, γ-PGA: siRNA = 5, w/w) by transmission electron microscope (scale bar = 100 nm). (F) Release behavior of siRNA from the gene complexes with or without GSH after 2 h-incubation. (G) Agarose gel electrophoresis of γ-PGA/RVA/siRNA complexes at different γ-PGA: siRNA weight ratios (N/P 30). (H) Standard curve for release of ATRA at different concentrations. (I) The quantitative release profile of ATRA in the RVA self-assembly was analyzed by an ultraviolet spectrophotometer.

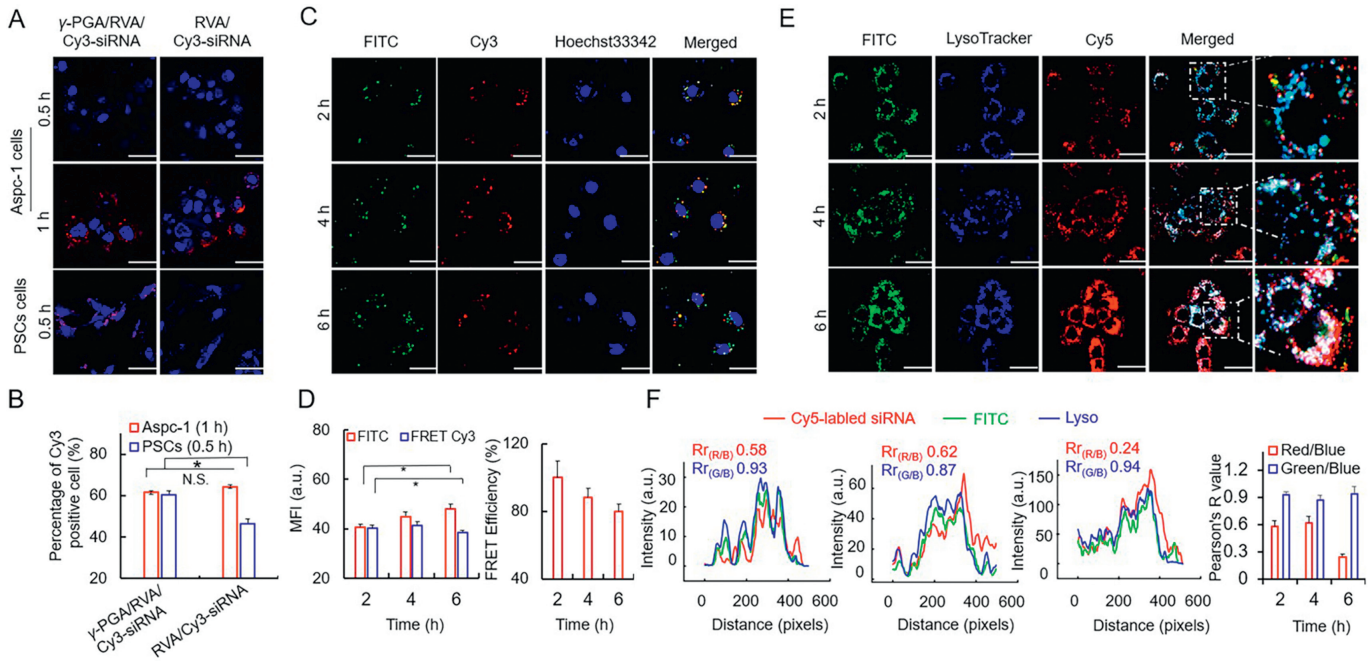

Fig. 3. Intracellular fate of different siRNA complexes in Aspc-1 or PSCs cells. (A) Cellular uptake at 0.5 and 1 h through confocal laser scanning microscopy (CLSM). Red fluorescence was provided by Cy3-labeled siRNA, and blue fluorescence was provided by Hoechst 33342 stained nuclei. Scale bar: 10 μm. (B) Flow cytometry analysis of Aspc-1/PSCs cells after incubation with Cy3-siRNA complexes for 0.5 or 1 h. (C) The dissociation of γ-PGA/RVA/siRNA complexes in Aspc-1 cells at different time points. Green: signal of FITC; Red: signal of FRET mediated Cy3; Blue: signal of Hoechst 33342 for cell nuclei staining; Yellow: the overlay signal of FRET Cy3 and FITC. Scale bar: 10 μm. (D) Semiquantitative fluorescence signals of FITC and FRET mediated Cy3, as well as corresponding FRET efficiency. The FRET efficiency was calculated according to the ratio of FITC to FRET mediated Cy3 signals. (E) CLSM images of Aspc-1 cell after incubation with Cy5-labeled siRNA complexes at different time points for endosomal escape assessment. Blue: signal of Lysotracker red, Green: signal of FITC, Red: signal of Cy5. (F) Pearson's correlation (Rr) calculation from CLSM images to evaluated endosomal release efficiency. $Rr_{(R/B)}$ and $Rr_{(G/B)}$ are calculated to express the colocalization degree of Cy5-siRNA and Lysotracker Red and the colocalization degree of FITC-γ-PGA and Lysotracker Red, respectively. Scale bars: 25 μm. $^{*}P < 0.05$, N.S.: no significance.

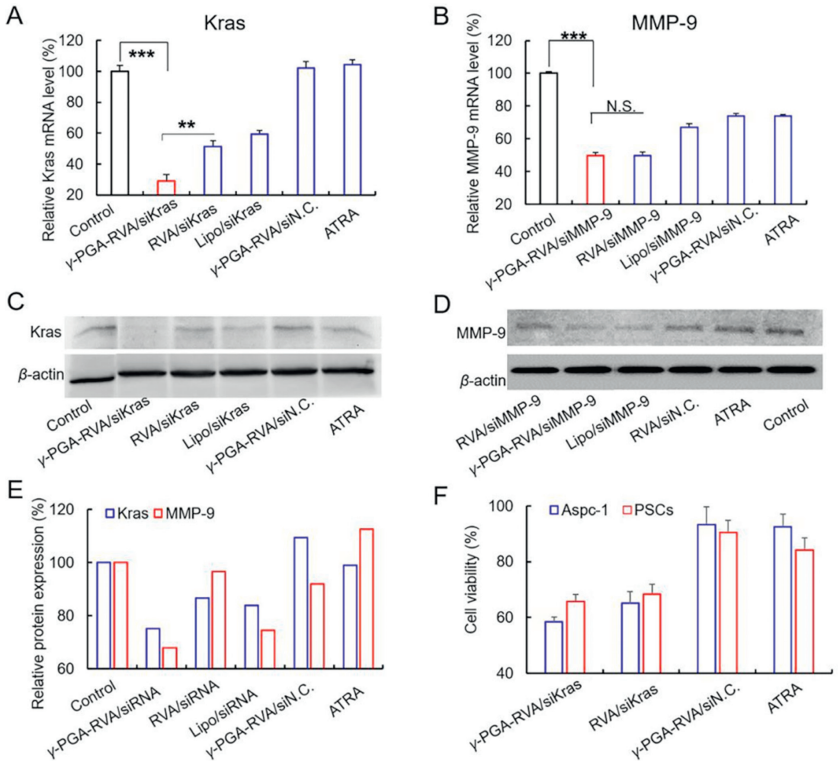

Fig. 4. Silence effect of siKras or siMMP-9 complexes in Aspc-1 cells: qRT-PCR analysis of Kras (A) or MMP-9 (B) suppression on transcriptional levels in Aspc-1 cells after treatment by different formulations for 24 h. Western blot analysis of Kras (C) or MMP-9 (D) suppression at protein levels in Aspc-1 cells after treatment with different formulations for 48 h. (E) Semi-analysis of Kras and MMP-9 protein expression as the ratio of target protein to reference gene of β-actin from immune blot results. (F) Cell viability of Aspc-1 and PSCs cells after treatment with various formulations for 48 h. $^{**}P < 0.01$, $^{***}P < 0.001$, N.S.: no significance.

by more than one-half at 6 h, as the gene complexes largely separated from the lysosome. In contrast, few changes were observed in Rr of signals from FITC-γ-PGA (green) and lysosome (blue). This suggested that γ-PGA is trapped in the lysosome after pH responsive disassociation from gene complexes.

As the delivery process has been confirmed unimpeded, we further utilized therapeutic siRNA of Kras (an oncogene with high mutation rate in pancreatic cancer) [30] and MMP-9 (a matrix metalloproteinase capable of regulate TME) [41] for incorporation effect evaluation on pancreatic cancer with this integrated delivery system. Kras is a carcinogenic gene with high mutation rate in pancreatic cancer [30]. We hypothesized that downregulation of Kras can synergistically work with the integrated all-*trans* retinoic acid in carrier materials to inhibit tumor more intuitively. MMP-9, is an important component of extracellular matrix, which participates in multiple processes of extracellular matrix [41]. Selection of it as the downregulation target gene could enhance the effect of micro-environment regulation, together with all-*trans* retinoic acid. First, the target gene silence efficiency was validated by quantitative real-time PCR (qRT-PCR) and Western Blot at both mRNA and protein levels (Fig. 4) on Aspc-1 cells. In general, the siRNA delivery efficiency of γ-PGA/RVA system is better than commercial gold standard Lipo2000. After γ-PGA/RVA/siRNA treatment, the expression of Kras decreased to 28.3% of the γ-PGA/RVA/siN.C., and that of MMP-9 mRNA declined to 49.8% (Figs. 4A and B). Meanwhile the silence efficiency of RVA/siKras and RVA/siMMP-9 binary gene complexes were relatively lower, with 50.4% and 53.7% respectively. The corresponding protein level evaluation also supported the above results. Silence effect of the γ-PGA/RVA/siRNA group was the most significant one (75.1% for Kras and 73.0% for MMP-9, respectively). In addition, compared with the γ-PGA/RVA/siN.C., ATRA itself has no effect on kras and MMP-9 gene expression (Figs. 4C-E).

The gene mutation in Kras causes function loss of molecular switch, which makes Kras protein always be in an activated state. And it activates many subsequent cellular processes such as tumor cell proliferation, transformation and invasion. The aim of killing tumor cell can be achieved by specifically silencing Kras gene with siRNA drug. Therefore, we investigated the inhibitory growth effect of siKras gene complexes on both pancreatic cancer cell (Aspc-1) and pancreatic stellate cell (PSCs) by CCK-8 analysis (Fig. 4F). Cell viability of Aspc-1 and PSCs declined to about 58.4% and 65.7% respectively, when compared to the group treated with γ-PGA/RVA/siN.C. Of note, ATRA has no significant effect on cell survival in both two kinds of cells.

Finally, the regulation effect of integrated co-delivery system on tumor microenvironment was studied. In normal pancreas, PSCs are in quiescent state with many lipid droplets containing vitamin A in the cytoplasm [42]. When the pancreatic cancer occurs, they would be activated, with disappearance of lipid droplets, overexpression of α-SMA (alpha-smooth muscle actin), secretion of a large amount of extracellular matrix (ECM) components (mainly denotes collagen I and fibronectin). The ECM components can expedite the development of pancreatic fibrosis and accelerate the occurrence of tumors by depositing collagen fibers [43,44]. Thus, the regulation evaluation was lied on lipid droplets formation, α-SMA expression, as well as collagen I and fibronectin secretion (Fig. 5).

In order to detect the reversion effect of ATRA conjugated in the RVA system, PSCs are firstly activated by the conditioned medium (mixture of Aspc-1 cells supernatant and fresh medium, v/v = 1:1). And with the help of florescent staining by Nile red, it was obvious that cells in ATRA containing groups (γ-PGA/RVA/siKras, γ-PGA/RVA/siMMP-9, γ-PGA/RVA/siN.C., ATRA) showed bright red fluorescence from droplets, due to the quiescent state restoration (Figs. 5A-D). Among them, free ATRA was the most efficient on

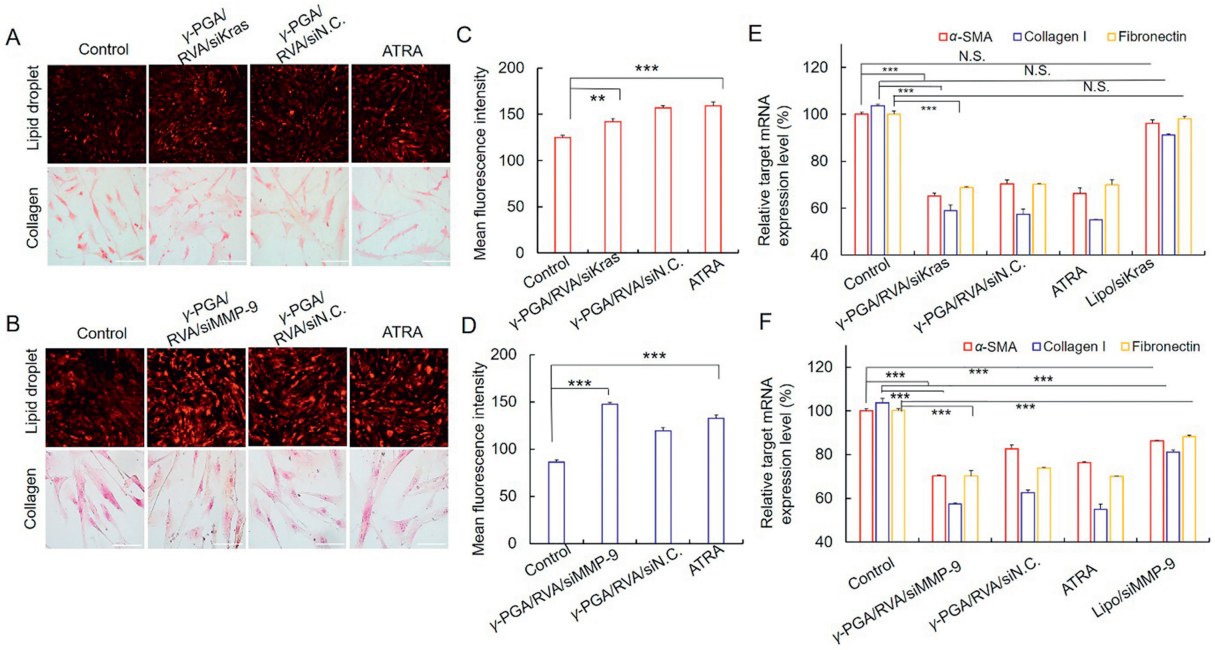

Fig. 5. Reversion of activated PSCs and TME regulation *in vitro*. (A, B) Nile red staining/Sirius red staining for lipid droplets/collagen I in the cytoplasm of PSCs cells with various treatments (scale bar = 75 μm). (C, D) The mean fluorescence intensity (MFI) of lipid droplet in different groups. (E, F) qPCR analysis for α-SMA, collagen I, fibronectin (markers of activated PSCs). $^{**}P < 0.01$, $^{***}P < 0.001$, N.S.: no significance.

cell reversion, which may attribute to the direct cellular uptake of lipidic ATRA without controlled release from the integrated compounds (Figs. 5A and B). Interestingly, siKras gene showed no effect on the lipid restoration, whereas siMMP-9 seems to promote it up to 20% (Figs. 5C and D). According to the published reports, MMP-9 can degrade collagen IV in the normal basement membrane, and then activate PSCs cells to promote the development of pancreatic cancer [45]. Therefore, we speculate that siMMP-9 and ATRA may synergistically reverse the activated PSCs cells to be quiescent [33,46].

Secretion of ECM components as well as the deposition of collagen I was detected. The mRNA level of α-SMA, collagen I and fibronectin in activated PSCs cells were all downregulated by ATRA containing reagents (γ-PGA/RVA/siKras, γ-PGA/RVA/siMMP-9, γ-PGA/RVA/siN.C., ATRA) at the same concentration of 5 μmol/L (Figs. 5E and F). Lipo/siKras with no effect on α-SMA expression illustrated that, Kras gene itself could neither regulate α-SMA gene, nor affect collagen I and fibronectin expression. So, the decreased secretion of ECM was primarily attributed to ATRA in these groups [33]. However, in group of Lipo/siMMP-9, the expression of α-SMA, collagen I and fibronectin exhibited a downward trend. It is probably because that MMP-9 itself can reverse the activated PSCs cells into a quiescent state [45,47]. After treatment with the ATRA containing complexes (γ-PGA/RVA/siKras, γ-PGA/RVA/siMMP-9, γ-PGA/RVA/siN.C., ATRA), the color of collagen I with Sirius red staining was much lighter than that in control, indicating less collagen I in these groups (Figs. 5A and B) [48].

These results indicated that the co-delivered ATRA achieved a successful reverse of active stromal PSCs with lipid droplets restoration and relative genes downregulation (α-SMA, collagen I and fibronectin). siRNA of oncogene Kras has no effect on the state turnover of activated PSCs, while siMMP-9 revealed the improved effect.

Results from *in vivo* fluorescence imaging showed that γ-PGA/RVA/siRNA most accumulated at tumor sites at various time points (2, 4, 8 and 24 h), compared with the free siRNA and RVA/siRNA group by tail vein injection (Fig. 6A). And *ex vivo*

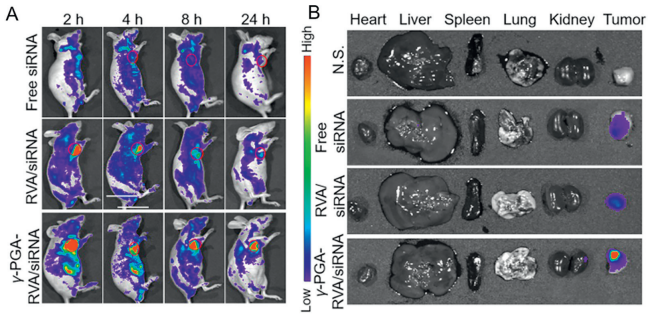

Fig. 6. *In vivo* targeting and distribution of gene complexes in heterotopic pancreatic cancer mice. (A) Representative *in vivo* imaging at 2, 4, 8 and 24 h after tail vein injection of free siRNA, RVA/siRNA, γ-RGA/RVA/siRNA respectively in mice with heterotopic pancreatic cancer. (B) Representative *ex vivo* images of tumor and major organs in heterotopic pancreatic cancer mice 24 h after injection (PBS, Free siRNA, RVA/siRNA and γ-RGA/RVA/siRNA.

imaging of dissected tissue after 24 h following injection also presented a similar result (Fig. 6B). The semi-quantitative results were consistent with the *in vitro* imaging results (Fig. S2 in Supporting information). Meanwhile, the increased tumor distribution reduced the corresponding non-specific accumulations in other investigated organs (heart, liver, spleen, lung and kidney). These data indicated that surface modification of γ-PGA on gene delivery system was benefit for more efficient tumor tissue targeting [36]. All animal experimental procedures were performed in accordance with the Guidelines for Care and Use of Laboratory Animals of West China Hospital of Sichuan University, and approved by the Biomedical Research Ethics Committee of West China Hospital of Sichuan University.

In conclusion, we have designed and synthesized an all-*trans* retinoic acid-based gene delivery system (γ-PGA/RVA), with target coating and sequential response to pH & redox stimuli. Combined with the siRNA (Kras, MMP-9), the system revealed capacity of killing pancreatic tumor cell and inactivating stromal cell coop-

eratively. The reasonable and ingenious integration design remarkably provided a facile but promising therapeutic strategy to refractory cancers, like pancreatic adenocarcinoma.

Declaration of competing interest

The authors have no conflict of interest.

Acknowledgments

This work was financially supported by National Natural Science Foundation of China (NSFC, Nos. 81873921 and 51903174), Sino-German Cooperation Group Project (No. GZ1512), China Postdoctoral Science Foundation (No. 2021M702772), Chengdu Science and Technology Program (No. 2020-GH02-00007-HZ), Sichuan University Postdoctoral Interdisciplinary Innovation Startup Foundation and the Fundamental Research Funds for Central Universities (No. 2021SCU12070).

Supplementary materials

Supplementary material associated with this article can be found, in the online version, at doi:10.1016/j.cclet.2022.107753.

References

[1] K. Lundstrom, Genes (Basel) 10 (2019) 189–212.
[2] U. Sahin, P. Oehm, E. Derhovanessian, et al., Nature 585 (2020) 107–112.
[3] C. Zhang, Q.T. Wang, H. Liu, Z.Z. Zhang, W.L Huang, Chin. J. Cancer 30 (2011) 182–188.
[4] T. Wu, Y. Dai, Cancer Lett. 387 (2017) 61–68.
[5] J. Hu, X. Yuan, F. Wang, et al., Chin. Chem. Lett. 32 (2021) 1341–1347.
[6] S. Hegde, V.E. Krisnawan, B.H. Herzog, et al., Cancer Cell 37 (2020) 289–307.
[7] J. Jiang, J. Mei, S. Yi, et al., Adv. Drug Delivery Rev. 180 (2022) 114046.
[8] Y. Li, T. Mei, S. Han, et al., Chin. Chem. Lett. 31 (2020) 3027–3040.
[9] J. Liao, Y. Jia, Y. Wu, et al., Wiley Interdiscip. Rev.: Nanomed. Nanobiotechnol. 12 (2020) e1581.
[10] Y. Lv, C. Xu, X. Zhao, ACS Nano 12 (2018) 1519–1536.
[11] E.F. Carapuca, E. Gemenetzidis, C. Feig, et al., J. Pathol. 239 (2016) 286–296.
[12] H.M. Kocher, B. Basu, F.E.M. Froeling, et al., Nat. Commun. 11 (2020) 4841.
[13] A. Hu, X. Chen, Q. Bi, et al., Nanoscale 12 (2020) 22615–22627.
[14] D. Guimaraes, A. Cavaco-Paulo, E. Nogueira, Int. J. Pharm. 601 (2021) 120571.
[15] L. Huang, S. Zhao, F. Fang, et al., Biomaterials 268 (2021) 120557.
[16] Y. Xiao, K. Shi, Y. Qu, B. Chu, Z. Qian, Mol. Ther. Methods Clin. Dev. 12 (2019) 1–18.
[17] H. Liang, Q. Bi, A. Hu, et al., Chem. Commun. 56 (2020) 6949–6952.
[18] J. Guo, L. Huang, Adv. Drug Delivery Rev. 156 (2020) 23–39.
[19] Z. Shi, Q. Li, L. Mei, Chin. Chem. Lett. 31 (2020) 1345–1356.
[20] X. He, Y. Hao, B. Chu, et al., Nano Today 39 (2021) 101174.
[21] B. Chu, Y. Qu, X. He, et al., Adv. Funct. Mater. 30 (2020) 2005918.
[22] Q. Jiang, Y. Nie, X. Chen, et al., Adv. Funct. Mater. 27 (2017) 1701571.
[23] Y. He, Y. Nie, G. Cheng, et al., Adv. Mater. 26 (2014) 1534–1540.
[24] X. Chen, J. Yang, H. Liang, et al., J. Mater. Chem. B 5 (2017) 1482–1497.
[25] X. Xu, Q. Jiang, X. Zhang, et al., J. Mater. Chem. B 3 (2015) 7006–7010.
[26] X. Chen, R. Jin, Q. Jiang, et al., Small 17 (2021) e2100609.
[27] F.E. Froeling, C. Feig, C. Chelala, et al., Gastroenterology 141 (2011) 1486–1497.
[28] Z.X. Liao, S.F. Peng, Y.C. Ho, et al., Biomaterials 33 (2012) 3306–3315.
[29] F. Xu, H. Zhong, Y. Chang, et al., Biomaterials 158 (2018) 56–73.
[30] Z. Fan, K. Fan, C. Yan, et al., Transl. Cancer Res. 7 (2018) 1728–1736.
[31] C.P. Hinzman, L. Aljehane, J.D. Brown-Clay, et al., Carcinogenesis 39 (2018) 1548–1559.
[32] J. Li, B. Chen, G.F. Fellows, C.G. Goodyer, R. Wang, Front. Cell Dev. Biol. 9 (2021) 694276.
[33] X. Han, Y. Li, Y. Xu, et al., Nat. Commun. 9 (2018) 3390.
[34] A. Tamura, N. Yui, Biomaterials 34 (2013) 2480–2491.
[35] X. Cheng, H.D. Xu, H.H. Ran, G. Liang, F.G. Wu, ACS Nano 15 (2021) 8039–8068.
[36] P.N. Brennan, J.F. Dillon, E.B. Tapper, Liver Int. 42 (2022) 9–15.
[37] S. Xue, X. Liu, S.L. Chen, W. Gan, Q. Yuan, Phys. Chem. Chem. Phys. 21 (2019) 26598–26605.
[38] A. Ajayaghosh, V.K. Praveen, C. Vijayakumar, Chem. Soc. Rev. 37 (2008) 109–122.
[39] D. Sharma, N.N.M. Rao, S. Arasaretnam, A.V. Sesha Sainath, M. Dhayal, Colloid Polym. Sci. 298 (2020) 365–375.
[40] S. Wang, Y. Tian, W. Tian, et al., ACS Nano 10 (2016) 8578–8590.
[41] Y.H. Cheng, E.I. Chiang, J.N. Syu, et al., PLoS One 16 (2021) e0247550.
[42] S.P. Pothula, R.C. Pirola, J.S. Wilson, M.V. Apte, Pancreatology 20 (2020) 409–418.
[43] A. Masamune, T. Watanabe, K. Kikuta, T. Shimosegawa, Clin. Gastroenterol. Hepatol. 7 (2009) S48–S54.
[44] A. Masamune, T. Shimosegawa, J. Gastroenterol. 44 (2009) 249–260.
[45] A. Venkateshwari, K. Sri Manjari, D. Krishnaveni, et al., Indian J. Clin. Biochem. 26 (2011) 136–139.
[46] B. Qian, L. Wei, Z. Yang, et al., Biomed. Pharmacother. 121 (2020) 109355.
[47] H. Huang, Sensors (Basel) 18 (2018) 3249.
[48] K. Koikawa, K. Ohuchida, S. Takesue, et al., Cancer Lett. 412 (2018) 143–154.